Rapid Communications

Ground states of Au_2Pb and pressure-enhanced superconductivity

Juefei Wu,[1,*] Zili Feng,[2,3,*] Jinghui Wang,[1] Qun Chen,[1] Chi Ding,[1] Tong Chen,[1] Zhaopeng Guo,[1] Jinsheng Wen,[1] Youguo Shi,[2,3] Dingyu Xing,[1] and Jian Sun[1,†]

[1]*National Laboratory of Solid State Microstructures, School of Physics and Collaborative Innovation Center of Advanced Microstructures, Nanjing University, Nanjing 210093, China*

[2]*Beijing National Laboratory for Condensed Matter Physics and Institute of Physics, Chinese Academy of Sciences, Beijing 100190, China*

[3]*Center of Materials Science and Optoelectronics Engineering, University of Chinese Academy of Sciences, Beijing 100049, China*

(Received 6 May 2019; published 12 August 2019)

Au_2Pb is a candidate of natural topological superconductors that has attracted much attention in the last few years. Combining *ab initio* calculations with machine-learning accelerated crystal structure searches, we have found two ground states of Au_2Pb: $Pca2_1$ phase at ambient pressure and $I\bar{4}2d$ phase at high pressure. The $Pca2_1$ phase is energetically more favorable than the known *Pbcn* structure and can be a candidate for x-ray diffraction refinement; our calculations suggest that high-pressure $I\bar{4}2d$ is a conventional superconductor. By the high-pressure electric resistance measurements, we observed evidence of a T_c enhancement. T_c reaches a maximum value of around 4 K at 5 GPa, then decreases with further compression. The superconductivity can remain unchanged after pressure releasing, in line with our theoretical predictions. These results show that Au_2Pb exhibits abundant behaviors under varied pressure and temperature, which can help to understand how to adjust its electronic properties by pressure.

DOI: 10.1103/PhysRevB.100.060103

Since the discovery of the strong spin-orbit coupling (SOC) induced topological insulators (TIs), topology has extended to more universal systems in physics [1], triggering tremendous research interests in topological materials in recent years [2–5]. The most typical topological materials are the topological insulators. TIs preserve a Z_2 invariant and the time-reversal symmetry protected helical edge states or Dirac cone surface states, as seen in HgTe quantum wells [6] and Bi_2Se_3 [7]. The second type is the nodal systems. The bulk gap closes at particular k points in the Brillouin zone, and the spatial lattice symmetries such as rotation or reflection play a significant role. They form Dirac cones, Fermi arcs, or flat bands. Such systems include Dirac semimetals [8,9], Weyl semimetals [10,11], and nodal line semimetals [12,13]. There are other types of new fermions or high-order topological states [14,15]. In addition, topological superconductors (TSCs) [16,17] are another fancy material which has both topological and superconducting properties.

Similar to the Dirac fermions on the surface, the bulk system of TSCs has a pairing gap, while the boundaries support gapless Majorana modes [3]. Achieving Majorana fermions is significant because of their novelty in condensed matter physics, and their potential applications in topological quantum computations. The basic idea to achieve TSCs is to realize an unconventional pairing symmetry for a topologically nontrivial state [4]. Even though several topological materials have superconductivity under ambient condition, such as $PbTaSe_2$ [18], the extreme rareness of TSCs calls for more routines. Successful routines include the using of proximity effect [19,20], doping [21], or pressurizing [22,23]. To use proximity effect is to fabricate a thin layered TI-superconductor heterostructure, such as the TI thin film Bi_2Se_3 coated on $NbSe_2$ [24]. A typical example of doping is the copper-doped topological insulator Bi_2Se_3 ($Cu_xBi_2Se_3$) [21–26]. $Cu_xBi_2Se_3$ is a TSC and its superconducting transition temperature (T_c) is 3.8 K [21–26]. But the interface interactions of the heterostructure bring complications to the system; the doping approach is hard to control, and can introduce disorder to the system. In addition, high pressure is an effective approach to alter the properties of topological materials, such as in Na_3Bi [27] and TaAs [28]. The pressure-induced superconductivity was observed in high-pressure experiments for several topological insulators (Bi_2Se_3 [29], Bi_2Te_3 [23], $ZrTe_5$ [30], Bi_4I_4 [31]) and Weyl semimetals (WTe_2 [32], TaP [33]).

Au_2Pb is a candidate natural TSC at ambient pressure [34–39]. The room temperature phase of Au_2Pb under ambient pressure is a cubic Laves phase (symmetry $Fd\bar{3}m$). First-principle calculations suggest that this $Fd\bar{3}m$ structure has a bulk Dirac cone along the Γ-X line protected by C_4 rotation symmetry. The angle-resolved photoemission spectroscopy (ARPES) experiments have confirmed the Dirac cone [38]. As the temperature drops, Au_2Pb undergoes several structural transitions, and the final ground state is an orthorhombic structure [34]. The low-temperature phase (symmetry suggested to be *Pbcn*) is superconducting ($T_c \sim 1.2$ K), and topologically nontrivial [35,37]. As revealed by point-contact measurement, if probing with harder tungsten (W) tip, T_c^{onset} could enhance to 2.1 K. Uniaxial pressure could be the main cause for such enhancement [36,39]. In addition, the cooling curves of the resistivity from 0 to 1.83 GPa indicate a high-pressure phase

*These authors contributed equally to this work.
†Corresponding author: jiansun@nju.edu.cn

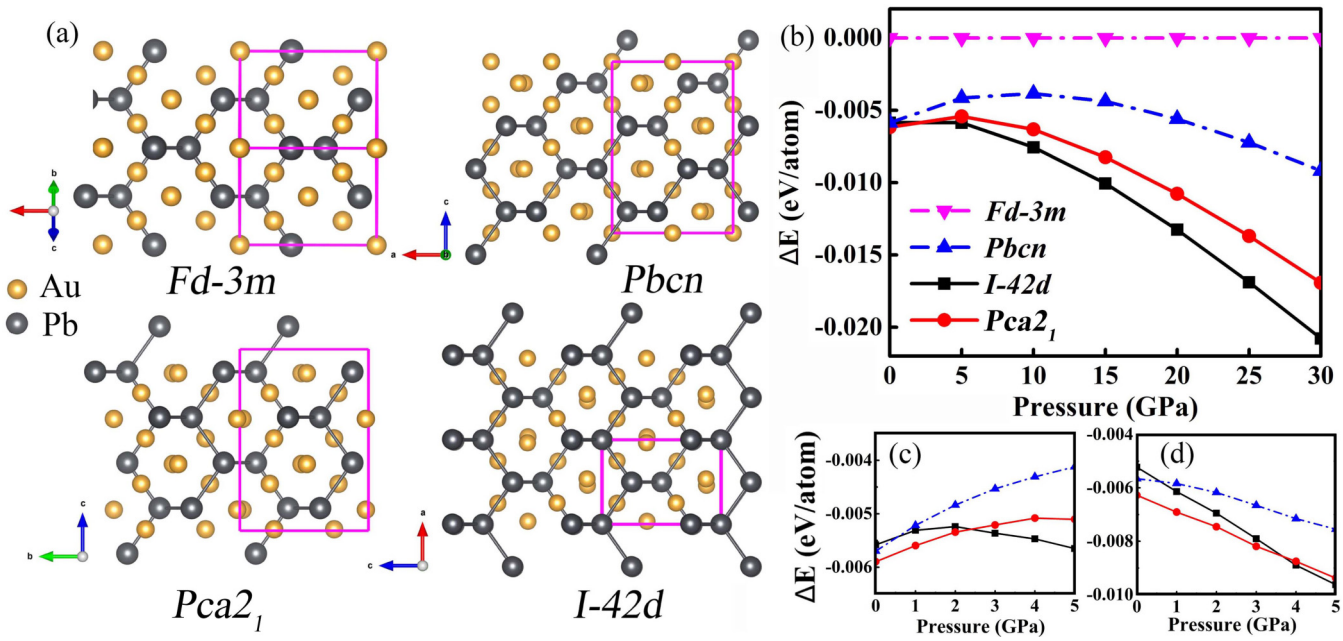

FIG. 1. (a) Crystal structures of Au_2Pb: the high-temperature phase $Fd\bar{3}m$; known low-temperature phase *Pbcn*; the predicted structures $Pca2_1$ and $I\bar{4}2d$. They have similar frameworks, but belong to different versions of the cubic Laves structure. The golden and gray balls represent Au and Pb atoms, respectively. (b) The pressure-dependent enthalpy difference relative to $Fd\bar{3}m$ using GGA-PBE. (c) The enthalpy difference among *Pbcn*, $Pca2_1$, and $I\bar{4}2d$ from 0 to 5 GPa using GGA-PBE. The enthalpy difference calculation is rechecked by (d) SCAN meta-GGA.

[35]. But it is still unknown what structure this high-pressure phase is and whether superconductivity remains. Thus, Au_2Pb possesses abundant structural properties. It provides a natural platform to investigate the relationship between topological and superconducting properties under pressure.

In this work, we study the ground states, the pressure-induced phase transitions, and pressure-enhanced superconductivity of Au_2Pb by combining *ab initio* calculations with high-pressure experiments. High-quality single crystals of Au_2Pb were grown and details are in the Supplemental Material [40]. The Au_2Pb powder was filled in a screw-pressure-type diamond-anvil cell made of nonmagnetic Cu-Be alloy without pressure medium, and in contact with four electronic probes. The high-pressure resistivity measurements were conducted in a physical property measurement system Quantum Design. Pressures were determined from the shift of the ruby fluorescence line [41].

Structure searches for Au_2Pb were performed using a machine-learning accelerated crystal structure prediction method [42] for different pressures. The structure optimization and enthalpy calculations were carried out using VASP [43–45] in the framework of density-functional theory with PBE-GGA functionals [46] and rechecked with SCAN meta-GGA [47]. We applied the PHONOPY [48] code to calculate the phonon dispersions. The electronic properties were calculated using WIEN2K [49]; the topological properties were investigated with the WANNIER90 [50–52] and WANNIERTOOLS [53] codes; and the electron-phonon coupling calculations were performed using the QUANTUM ESPRESSO package [54]. More details are in the Supplemental Material [40].

We performed structure searches at 10, 20, and 50 GPa. The known $Fd\bar{3}m$ structure and *Pbcn* structure [Fig. 1(a)] were treated as seeds during the structure searches. After tens of generations, we picked out an orthorhombic structure $Pca2_1$ and a tetragonal structure $I\bar{4}2d$ [Fig. 1(a)]. As shown in Fig. 1(a), the predicted $Pca2_1$ and $I\bar{4}2d$ structures are different versions of the cubic Laves phase structure. The positions of Au atoms and the lattice parameters cause different distortions among these structures. Detailed lattice parameters are listed in Supplemental Material Table S1.

The enthalpy-pressure relation is plotted in Fig. 1(b). The high-temperature phase $Fd\bar{3}m$ has the highest value in the whole pressure range. Below 2 GPa, the enthalpy of the predicted $Pca2_1$ structure is lower than the known *Pbcn* structure. When the pressure is above 2 GPa, the predicted $I\bar{4}2d$ structure is more energetically stable. We rechecked the enthalpy with SCAN meta-GGA [47] [Fig. 1(d)] because the energy between the predicted $Pca2_1$ structure and the known *Pbcn* structure is less than 1 meV/atom at lower pressure. The enthalpy value of the predicted $Pca2_1$ structure is still less than that of the *Pbcn* structure using SCAN meta-GGA, and the transition pressure from the $Pca2_1$ phase to the $I\bar{4}2d$ phase becomes around 4 GPa. We further calculate the phonon dispersions of the known *Pbcn* structure and the predicted $Pca2_1$ structure at ambient pressure. As shown in Figs. 2(a) and 2(b), the phonon curves of the known *Pbcn* structure have imaginary frequencies, while our predicted $Pca2_1$ structure has no imaginary value, illustrating that $Pca2_1$ is more dynamically stable. By comparing the simulation x-ray diffraction (XRD) curves [55] (more details are in Supplemental Material Figs. S2 and S3) with the experiment results, we find that both simulation curves match well with the experiment data. The wavelength $\lambda = 0.4138$ Å is the same as the one used in Ref. [34]. Further comparing the lattice parameters, the

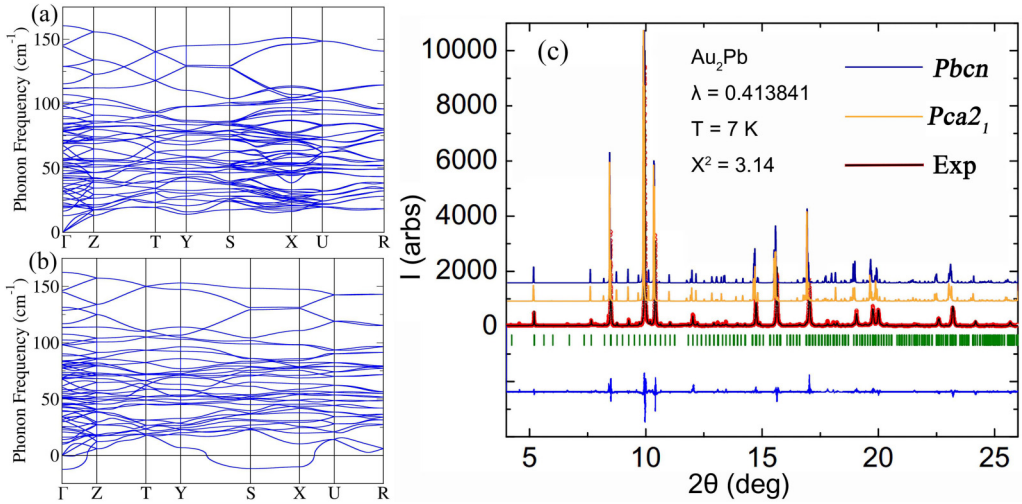

FIG. 2. The phonon curves of the (a) $Pca2_1$ and (b) *Pbcn* structures calculated at 0 GPa. There is no imaginary frequency for $Pca2_1$, while *Pbcn* has imaginary phonon modes. (c) The simulation XRD pattern of $Pca2_1$ and *Pbcn* compared with the experiment results. The experimental data are from Ref. [35]. The $Pca2_1$ simulation curves match well with the experiment curves, suggesting that the previous experiment [35] is possible to explain by the predicted $Pca2_1$ structure.

difference between the XRD experimental value [34] and the calculated results of the predicted $Pca2_1$ is less than 1% using SCAN meta-GGA. The SCAN meta-GGA result is more accurate than the GGA-PBE result (2.5% larger in the c axis than the experimental value). This shows the reliability of SCAN meta-GGA, and the possibility to refine the XRD data with the predicted $Pca2_1$ structure. Thus, we recommend the predicted $Pca2_1$ structure for future XRD refinement, and we believe that the $Pca2_1$ structure is more likely to be the ground state of Au_2Pb under ambient pressure.

The electronic structure of $Pca2_1$ is calculated with and without SOC [see Figs. S1(a) and S1(b)]. Considering SOC, the band structure crossings along the Γ-Z and T-Y paths open a gap of over 40 meV. $Pca2_1$ is a noncentrosymmetric semimetal, while *Pbcn* has an inversion center. We calculated the $\mathbb{Z}_2$ invariant via Wannier charge centers with the help of maximally localized Wannier functions (MLWFs) [53]. The $\mathbb{Z}_2$ invariant for the $Pca2_1$ phase is $(v_0 : v_1v_2v_3) = (1 : 010)$, illustrating that the predicted $Pca2_1$ structure is topologically nontrivial. Even though the overall surface states are complicated, we can get the surface state along the Z-T direction [see Fig. S1(c)]. ARPES experiments can detect surface states and may provide more evidence for structure determination. We did not carry out the electron-phonon coupling (EPC) calculation of $Pca2_1$, because the unit cell has 24 heavy atoms, which makes the cost unaffordable at the current stage.

According to the calculated results from SCAN meta-GGA, the predicted tetragonal $I\bar{4}2d$ structure becomes more energetically favorable when the pressure is above 4 GPa [Fig. 1(d)]. Both of the calculated phonon curves of $I\bar{4}2d$ at 10 GPa and ambient pressure have no imaginary frequency (Fig. S4), suggesting the $I\bar{4}2d$ structure is dynamically stable. Hence, $I\bar{4}2d$ is not only stable at high pressure but can stay dynamically stable after pressure releasing. As seen by the band structure depicted in Fig. S5, the nodal line in the Z-Γ-X plane opens a gap (∼25 meV) because of SOC. There is always a direct gap along the k-point path in Fig. S5 for the $I\bar{4}2d$ structure, which suggests the possibility of nontrivial properties. With the help of MLWFs, the $\mathbb{Z}_2$ invariant for the $I\bar{4}2d$ structure is $(v_0 : v_1v_2v_3) = (0 : 000)$. Further calculating the Berry phase, irreducible representations, and the charge chirality at specific k points, we find that $I\bar{4}2d$ is topologically trivial.

To study the potential superconductivity of $I\bar{4}2d$, we perform EPC calculations with density-functional perturbation theory at different pressures. Phonon dispersions, phonon density of states, the corresponding Eliashberg spectral function $\alpha^2F(\omega)$, and the EPC parameter λ as a function of frequency for the $I\bar{4}2d$ structure are calculated at 5 GPa, and the results are shown in Fig. 3(a). The resulting integral λ and logarithmic average phonon frequencies ($\omega_{\log}$) are calculated using the Eliashberg formalism. T_c values are estimated using the Allen-Dynes modified McMillan equation [56] with typical Coulomb pseudopotential parameters $\mu^* = 0.1$. We also apply $\mu^* = 0.13$ according to Ref. [34] (Supplemental Material Table S2). In the pressure range, T_c has a peak at 5 GPa [Fig. 3(b)]. The calculated T_c at 5 GPa is 5.04 and 4.17 K for $\mu^* = 0.1$ and 0.13, respectively. To further understand the peak of calculated T_c at 5 GPa, we compare the density of states (DOS) [Fig. S7(a)], phonon density of states (PHDOS) [Fig. S7(b)], Fermi surfaces [Figs. S6(c) and S6(d)], and the corresponding band structures [Figs. S6(a) and S6(b)] at 5 and 0 GPa. The PHDOS exhibit hardening behavior, which corresponds to the decrease of T_c, while the DOS are enhanced around the Fermi level. As shown in Fig. S6, a hole-type Fermi pocket emerges around the Z point at 5 GPa, in line with the DOS results. This new Fermi pocket may play a key role in the T_c enhancement at 5 GPa.

Based on the above calculations, we performed high-pressure experiments to further study our theoretical predictions. We found evidence for pressure-enhanced superconductivity. Using different powder samples in run 1 and run 2, we observed superconductivity in both run 1 and run 2. In run 1, resistivity was measured at different pressures

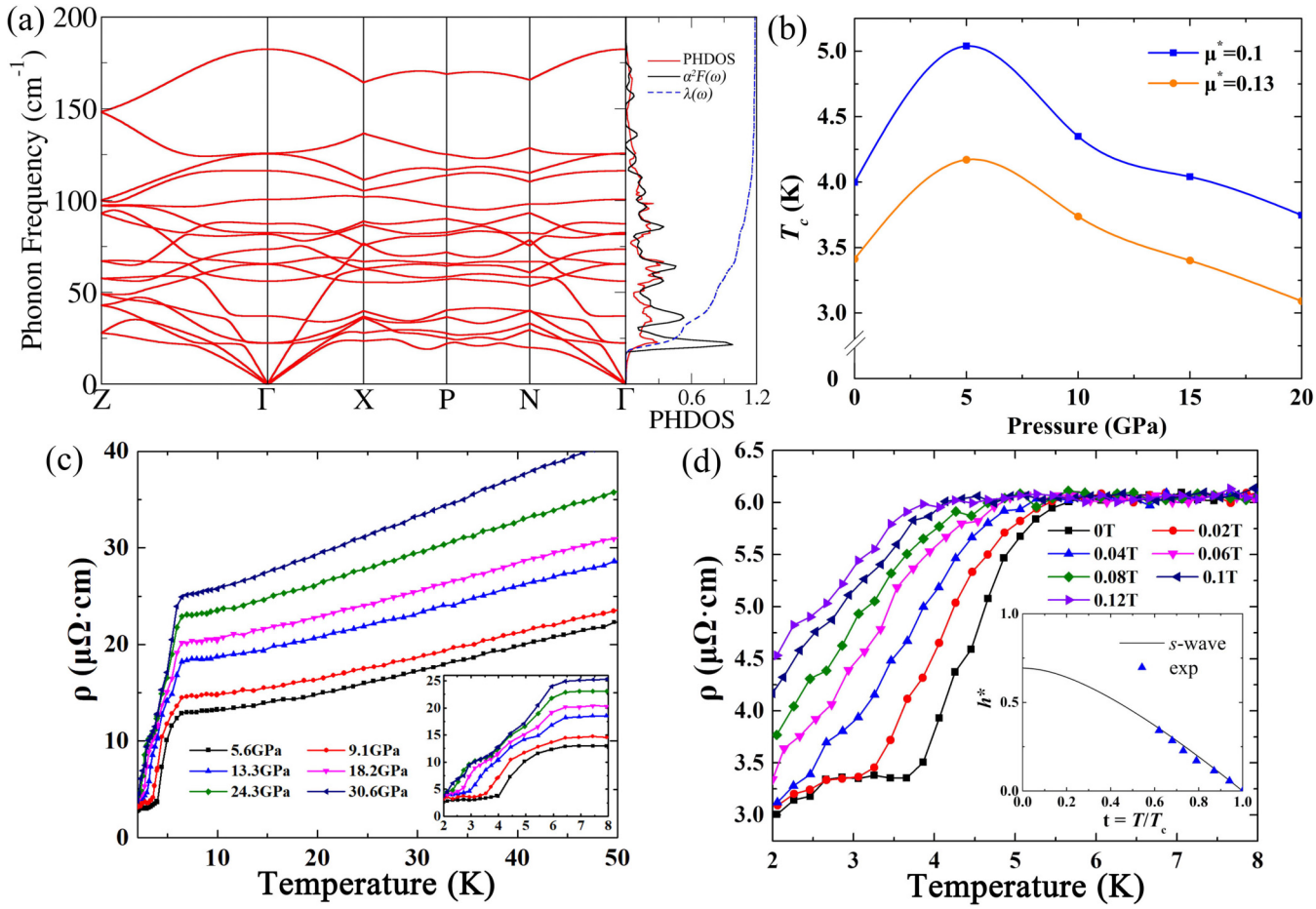

FIG. 3. (a) Calculated phonon dispersion curves, phonon density of states (PHDOS), Eliashberg EPC spectral function $\alpha^2F(\omega)$, and electron-phonon integral $\lambda(\omega)$ of $I\bar{4}2d$ at 5 GPa. (b) The calculated pressure dependence of T_c for $I\bar{4}2d$ from 0 to 20 GPa with different μ^*. (c) The resistivity of Au_2Pb for various pressures as a function of temperature from 5 to 30 GPa in run 1. The inset shows the detailed ρ-T curves from 2 to 8 K. (d) The resistivity as a function of temperature for Au_2Pb applied with different magnetic field at 6.5 GPa in run 2. T_c is suppressed with the increasing magnetic field. The inset compares the normalized critical field h^* (blue squares) to the s-wave superconductor model (black line).

in pressure-increasing and -releasing processes. In run 2, the resistivity was measured under various magnetic fields at 6.5 GPa. Figure 3(c) shows the temperature-dependent resistivity $\rho(T)$ at pressures from 5 to 30 GPa in run 1; all the curves show metallic behavior. Resistivity has a sharp drop around 6 K at 5.6 GPa. After a drop by an order of magnitude, the resistivity remains constant around 4 K, which is determined as the superconducting transition temperature, T_c. The residual resistivity below T_c is likely owing to the nonhydrostatic pressure condition and the corresponding incomplete structure transition around the sample's fringe area [57]. When the pressure further increases, T_c monotonically decreases to about 2 K at 24.3 GPa, and the upper critical field H_{c2} decreases with pressure, as presented in Fig. S8. In run 2, the pressure-induced superconductivity is further corroborated by the resistivity measurements under external magnetic fields. Figure 3(d) displays $\rho(T)$ at 6.5 GPa in run 2 under various magnetic fields up to 0.12 T. The magnetic field is perpendicular to the diamond culet. T_c is suppressed and shifts to a lower temperature with increasing magnetic field. Using a similar method to that applied in Refs. [37,57], we further investigate the critical temperature T_c (here is the onset of the resistance drop) dependence of the upper critical field H_{c2} [Fig. 3(d)]. The H_{c2} results have a linear dependence of temperature, and the data reveals $dH_{c2}(T)/dT_c = -0.0645$ T/K near T_c. It is common to compare the H_{c2} data with known models. We calculated the reduced critical field with $h^*(T) = [H_{c2}/T_c]/[dH_{c2}/dT|_{T=Tc}]$, then compared it to the model for s-wave superconductors [Werthamer-Helfand-Hohenberg theory (WHH) [58], $H_{c2} \approx 0.7T_c \times dH_{c2}/dT|_{T=Tc}$, or $h^*(0) \approx 0.7$). As shown in the inset of Fig. 3(d), our experimental measured data follow the behavior of the s-wave superconductor model, suggesting the high-pressure phase of Au_2Pb to be a conventional superconductor. The pressure decreasing results in run 1 are shown in Fig. S9. T_c recovers to 3.73 K at 9.4 GPa and remains almost constant with further decompression;for instance, $T_c = 3.53$ K at 0.85 GPa, suggesting that the high-pressure phase is likely to exist after pressure releasing. The T_c result after pressure releasing is close to the calculated $T_c = 3.41$ K for $I\bar{4}2d$ at 0 GPa with $\mu^* = 0.13$. In addtion, the overall T_c results match with our calculated values for $I\bar{4}2d$ (Supplemental Material Table S2). The experiment phenomenon agrees with our theoretical calculation of $I\bar{4}2d$. Our results provide evidence of the pressure-enhanced

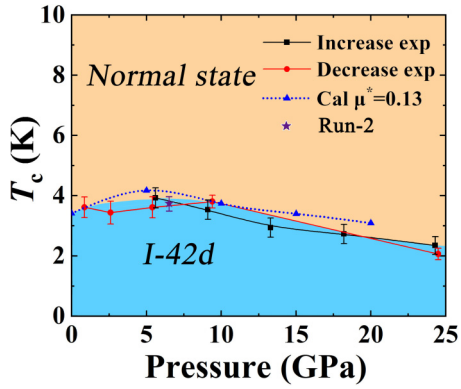

FIG. 4. Superconducting phase diagram of Au_2Pb with the $I\bar{4}2d$ structure. The blue region corresponds to the superconducting phase and the orange region corresponds to the normal state. The black squares represent the measured values of T_c in the pressure-increasing process of run 1; the red circles are those in the pressure-releasing process of run 1; the purple pentagram represents the T_c under 0 T in run 2 and the blue triangles represent the calculated values of T_c with $\mu^* = 0.13$.

superconductivity of Au_2Pb; we attribute the high-pressure behavior of Au_2Pb to our predicted high-ressure phase $I\bar{4}2d$. It still requires more evidence to illustrate the high-pressure transition properties of the Au_2Pb, e.g., careful x-ray diffraction and more explicit resistivity measurements under high pressure.

As shown in Fig. 4, we summarize the characteristic parameters (T_c and P) in a superconducting phase diagram for the high-pressure phase of Au_2Pb. The phase transition pressure is between 4 and 5 GPa according to SCAN meta-GGA. T_c reaches a maximum of nearly 4 K at around 5.6 GPa, then gradually decreases with further compression. After pressure releasing, the high-pressure phase remains unchanged, and T_c is 3.53 K at 0.85 GPa, agreeing with the theoretical calculation of $I\bar{4}2d$. In run 2, the T_c is 3.74 K at 6.5 GPa, and T_c decreases with increasing magnetic field. Our calculated value for T_c of $I\bar{4}2d$ at ambient pressure is 3.41 K ($\mu^* = 0.13$), which is in line with the high-pressure experimental result.

In summary, we have three conclusions from our *ab initio* calculations and high-pressure experiments. First, we predict two new ground states of Au_2Pb: $Pca2_1$ phase at ambient pressure and $I\bar{4}2d$ phase at high pressure. The predicted $Pca2_1$ is topologically nontrivial and dynamically stable. It has a lower energy, thus the ground state of Au_2Pb at ambient pressure is more likely to be the $Pca2_1$ structure instead of the *Pbcn* structure. We recommend further XRD refinement in the future. Second, in the high-pressure experiments, we find evidence of pressure-enhanced superconductivity above 5 GPa. The superconductivity remains even after pressure releasing. The overall behavior of Au_2Pb under high pressure matches well with our predicted high-pressure $I\bar{4}2d$ structure. In addition, our calculation suggests such structural transition accompanies a topological phase transition, because the $I\bar{4}2d$ phase is topologically trivial while the ambient phase is nontrivial. Lastly, the $I\bar{4}2d$ structure is a conventional BCS superconductor. Its T_c maximum (≈ 4 K, at around 5 GPa) is about three times more than that of the $Pca2_1$ or *Pbcn* structure. The pressure-induced superconductivity was first seen in Au_2Pb, and the pressure dependences of T_c from our theoretical calculations and experiments align well with each other.

We thank Huaiqiang Wang for the help with the fitting of the WHH model. We acknowledge financial support from the MOST of China (Grants No. 2016YFA0300404 and No. 2015CB921202) and from the NSFC (Grants No. 11574133, No. 11834006, No. 11822405, and No. 11774399), the Fundamental Research Funds for the Central Universities and the K. C. Wong Education Foundation (GJTD-2018-01). Calculations were performed on the supercomputer in the High Performance Computing Center of Collaborative Innovation Center of Advanced Microstructures, the High Performance Computing Center of Nanjing University, and "Tianhe-2" at NSCC-Guangzhou.

[1] O. Vafek and A. Vishwanath, Annu. Rev. Condens. Matter Phys. **5**, 83 (2014).
[2] M. Z. Hasan and C. L. Kane, Rev. Mod. Phys. **82**, 3045 (2010).
[3] X. L. Qi and S. C. Zhang, Rev. Mod. Phys. **83**, 1057 (2011).
[4] C. K. Chiu, J. C. Y. Teo, A. P. Schnyder, and S. Ryu, Rev. Mod. Phys. **88**, 035005 (2016).
[5] A. Bansil, H. Lin, and T. Das, Rev. Mod. Phys. **88**, 021004 (2016).
[6] S. W. M. König, C. Brüne, A. Roth, H. Buhmann, L. W. Molenkamp, X. L. Qi, and S. C. Zhang, Science **318**, 766 (2007).
[7] L. Fu, Phys. Rev. Lett. **103**, 266801 (2009).
[8] Z. Wang, Y. Sun, X. Q. Chen, C. Franchini, G. Xu, H. Weng, X. Dai, and Z. Fang, Phys. Rev. B **85**, 195320 (2012).
[9] Z. K. Liu, J. Jiang, B. Zhou, Z. J. Wang, Y. Zhang, H. M. Weng, D. Prabhakaran, S. K. Mo, H. Peng, P. Dudin, T. Kim, M. Hoesch, Z. Fang, X. Dai, Z. X. Shen, D. L. Feng, Z. Hussain, and Y. L. Chen, Nat. Mater. **13**, 677 (2014).
[10] S. Xu, I. Belopolski, N. Alidoust, M. Neupane, G. Bian, C. Zhang, R. Sankar, G. Chang, Z. Yuan, C. Lee, S. Huang, H. Zheng, J. Ma, D. S. Sanchez, B. Wang, A. Bansil, F. Chou, P. P. Shibayev, H. Lin, S. Jia, and M. Z. Hasan, Science **349**, 613 (2015).
[11] B. Q. Lv, H. M. Weng, B. B. Fu, X. P. Wang, H. Miao, J. Ma, P. Richard, X. C. Huang, L. X. Zhao, G. F. Chen, Z. Fang, X. Dai, T. Qian, and H. Ding, Phys. Rev. X **5**, 031013 (2015).
[12] G. Bian, T. R. Chang, R. Sankar, S. Y. Xu, H. Zheng, T. Neupert, C. K. Chiu, S. M. Huang, G. Chang, I. Belopolski, D. S. Sanchez, M. Neupane, N. Alidoust, C. Liu, B. Wang, C. C. Lee, H. T. Jeng, C. Zhang, Z. Yuan, S. Jia, A. Bansil, F. Chou, H. Lin, and M. Z. Hasan, Nat. Commun. **7**, 10556 (2016).
[13] J. Hu, Z. Tang, J. Liu, X. Liu, Y. Zhu, D. Graf, K. Myhro, S. Tran, C. N. Lau, J. Wei, and Z. Mao, Phys. Rev. Lett. **117**, 016602 (2016).

[14] Z. Wang, A. Alexandradinata, R. J. Cava, and B. A. Bernevig, Nature (London) **532**, 189 (2016).

[15] W. A. Benalcazar, B. A. Bernevig, and T. L. Hughes, Science **357**, 61 (2017).

[16] L. Fu and C. L. Kane, Phys. Rev. Lett. **100**, 096407 (2008).

[17] C. W. J. Beenakker, Annu. Rev. Condens. Matter Phys. **4**, 113 (2013).

[18] M. N. Ali, Q. D. Gibson, T. Klimczuk, and R. J. Cava, Phys. Rev. B **89**, 020505(R) (2014).

[19] R. M. Lutchyn, J. D. Sau, and S. Das Sarma, Phys. Rev. Lett. **105**, 077001 (2010).

[20] A. Das, Y. Ronen, Y. Most, Y. Oreg, M. Heiblum, and H. Shtrikman, Nat. Phys. **8**, 887 (2012).

[21] Y. S. Hor, A. J. Williams, J. G. Checkelsky, P. Roushan, J. Seo, Q. Xu, H. W. Zandbergen, A. Yazdani, N. P. Ong, and R. J. Cava, Phys. Rev. Lett. **104**, 057001 (2010).

[22] H. Wang, H. Wang, H. Liu, H. Lu, W. Yang, S. Jia, X. J. Liu, X. C. Xie, J. Wei, and J. Wang, Nat. Mater. **15**, 38 (2016).

[23] J. L. Zhang, S. J. Zhang, H. M. Weng, W. Zhang, L. X. Yang, Q. Q. Liu, S. M. Feng, X. C. Wang, R. C. Yu, L. Z. Cao, L. Wang, W. G. Yang, H. Z. Liu, W. Y. Zhao, S. C. Zhang, X. Dai, Z. Fang, and C. Q. Jin, Proc. Natl. Acad. Sci. USA **108**, 24 (2011).

[24] S. Y. Xu, N. Alidoust, I. Belopolski, A. Richardella, C. Liu, M. Neupane, G. Bian, S. H. Huang, R. Sankar, C. Fang, B. Dellabetta, W. Dai, Q. Li, M. J. Gilbert, F. Chou, N. Samarth, and M. Z. Hasan, Nat. Phys. **10**, 943 (2014).

[25] L. A. Wray, S. Y. Xu, Y. Xia, Y. S. Hor, D. Qian, A. V. Fedorov, H. Lin, A. Bansil, R. J. Cava, and M. Z. Hasan, Nat. Phys. **6**, 855 (2010).

[26] S. Sasaki, M. Kriener, K. Segawa, K. Yada, Y. Tanaka, M. Sato, and Y. Ando, Phys. Rev. Lett. **107**, 217001 (2011).

[27] D. Shao, J. Ruan, J. Wu, T. Chen, Z. Guo, H. Zhang, J. Sun, L. Sheng, and D. Xing, Phys. Rev. B **96**, 075112 (2017).

[28] Y. Zhou, P. Lu, Y. Du, X. Zhu, G. Zhang, R. Zhang, D. Shao, X. Chen, X. Wang, M. Tian, J. Sun, X. Wan, Z. Yang, W. Yang, Y. Zhang, and D. Xing, Phys. Rev. Lett. **117**, 146402 (2016).

[29] K. Kirshenbaum, P. S. Syers, A. P. Hope, N. P. Butch, J. R. Jeffries, S. T. Weir, J. J. Hamlin, M. B. Maple, Y. K. Vohra, and J. Paglione, Phys. Rev. Lett. **111**, 087001 (2013).

[30] Y. H. Zhou, J. F. Wu, W. Ning, N. N. Li, Y. P. Du, X. L. Chen, R. R. Zhang, Z. H. Chi, X. F. Wang, X. D. Zhu, P. C. Lu, C. Ji, X. G. Wan, Z. R. Yang, J. Sun, W. G. Yang, M. L. Tian, Y. H. Zhang, and H. K. Mao, Proc. Natl. Acad. Sci. USA **113**, 2904 (2016).

[31] X. Wang, J. Wu, J. Wang, T. Chen, H. Gao, P. Lu, Q. Chen, C. Ding, J. Wen, and J. Sun, Phys. Rev. B **98**, 174112 (2018).

[32] P. Lu, J. S. Kim, J. Yang, H. Gao, J. Wu, D. Shao, B. Li, D. Zhou, J. Sun, D. Akinwande, D. Xing, and J. F. Lin, Phys. Rev. B **94**, 224512 (2016).

[33] Y. F. Li, Y. H. Zhou, Z. P. Guo, F. Han, X. L. Chen, P. C. Lu, X. F. Wang, C. An, Y. Zhou, J. Xing, G. Du, X. Y. Zhu, H. Yang, J. Sun, Z. R. Yang, W. G. Yang, H. K. Mao, Y. H. Zhang, and H. H. Wen, npj Quant. Mater. **2**, 66 (2017).

[34] L. M. Schoop, L. S. Xie, R. Chen, Q. D. Gibson, S. H. Lapidus, I. Kimchi, M. Hirschberger, N. Haldolaarachchige, M. N. Ali, C. A. Belvin, T. Liang, J. B. Neaton, N. P. Ong, A. Vishwanath, and R. J. Cava, Phys. Rev. B **91**, 214517 (2015).

[35] K. W. Chen, D. Graf, T. Besara, A. Gallagher, N. Kikugawa, L. Balicas, T. Siegrist, A. Shekhter, and R. E. Baumbach, Phys. Rev. B **93**, 045118 (2016).

[36] Y. Xing, H. Wang, C. K. Li, X. Zhang, J. Liu, Y. Zhang, J. Luo, Z. Wang, Y. Wang, L. Ling, M. Tian, S. Jia, J. Feng, X. J. Liu, J. Wei, and J. Wang, npj Quant. Mater. **1**, 16005 (2016).

[37] Y. J. Yu, Y. Xu, Y. Xing, J. Zhang, T. P. Ying, X. C. Hong, M. X. Wang, X. Zhang, S. Jia, J. Wang, and S. Y. Li, Europhys. Lett. **116**, 67002 (2016).

[38] Y. Wu, G. Drachuck, L. L. Wang, D. D. Johnson, P. Swatek, B. Schrunk, D. Mou, L. Huang, S. L. Bud'ko, P. C. Canfield, and A. Kaminski, Phys. Rev. B **98**, 161107 (2018).

[39] H. Wang, L. Ma, and J. Wang, Sci. Bull. **63**, 1141 (2018).

[40] See Supplemental Material at http://link.aps.org/supplemental/10.1103/PhysRevB.100.060103 for supplemental methods, crystal structures, electronic structures, phonon spectra, comparisons of x-ray diffraction patterns, measurements of superconducting properties, etc.

[41] H. K. Mao, J. Xu, and P. M. Bell, J. Geophys. Res. **91**, 4673 (1986).

[42] K. Xia, H. Gao, C. Liu, J. Yuan, J. Sun, H. T. Wang, and D. Xing, Sci. Bull. **63**, 817 (2018).

[43] G. Kresse and J. Furthmüller, Phys. Rev. B **54**, 11169 (1996).

[44] H. J. Monkhorst and J. D. Pack, Phys. Rev. B **13**, 5188 (1976).

[45] P. E. Blöchl, Phys. Rev. B **50**, 17953 (1994).

[46] J. P. Perdew, K. Burke, and M. Ernzerhof, Phys. Rev. Lett. **77**, 3865 (1996).

[47] J. Sun, A. Ruzsinszky, and J. P. Perdew, Phys. Rev. Lett. **115**, 036402 (2015).

[48] A. Togo, F. Oba, and I. Tanaka, Phys. Rev. B **78**, 134106 (2008).

[49] P. Blaha, K. Schwarz, G. K. H. Madsen, D. Kvasnicka, and J. Luitz, *WIEN2k, an Augmented Plane Wave Plus Local Orbitals Program for Calculating Crystal Properties* (Techn. Universität Wien, Austria, 2001).

[50] A. A. Mostofi, J. R. Yates, G Pizzi, Y. S. Lee, I. Souza, D. Vanderbilt, and N. Marzari, Comput. Phys. Commun. **185**, 2309 (2014).

[51] N. Marzari and D. Vanderbilt, Phys. Rev. B **56**, 12847 (1997).

[52] I. Souza, N. Marzari, and D. Vanderbilt, Phys. Rev. B **65**, 035109 (2001).

[53] Q. S. Wu, S. N. Zhang, H. F. Song, M. Troyer, and A. A. Soluyanov, Comput. Phys. Commun. **224**, 405 (2017).

[54] P. Giannozzi, S. Baroni, N. Bonini, M. Calandra, R. Car, C. Cavazzoni, D. Ceresoli, G. L. Chiarotti, M. Cococcioni, I. Dabo, A. Dal Corso, S. de Gironcoli, S. Fabris, G. Fratesi, R. Gebauer, U. Gerstmann, C. Gougoussis, A. Kokalj, M. Lazzeri, L. Martin-Samos, N. Marzari, F. Mauri, R. Mazzarello, S. Paolini, A. Pasquarello, L. Paulatto, C. Sbraccia, S. Scandolo, G. Sclauzero, A. P. Seitsonen, A. Smogunov, P. Umari, and R. M. Wentzcovitch, J. Phys.: Condens. Matter **21**, 395502 (2009).

[55] B. H. Toby and R. B. Von Dreele, J. Appl. Crystallogr. **46**, 544 (2013).

[56] P. B. Allen and R. C. Dynes, Phys. Rev. B **12**, 905 (1975).

[57] Z. Chi, X. Chen, F. Yen, F. Peng, Y. Zhou, J. Zhu, Y. Zhang, X. Liu, C. Lin, S. Chu, Y. Li, J. Zhao, T. Kagayama, Y. Ma, and Z. Yang, Phys. Rev. Lett. **120**, 037002 (2018).

[58] N. R. Werthamer, E. Helfand, and P. C. Hohenberg, Phys. Rev. **147**, 295 (1966).